Since January 2020 Elsevier has created a COVID-19 resource centre with free information in English and Mandarin on the novel coronavirus COVID-19. The COVID-19 resource centre is hosted on Elsevier Connect, the company's public news and information website.

Journal of Theoretical Biology 284 (2011) 142–148

Contents lists available at ScienceDirect

Journal of Theoretical Biology

journal homepage: www.elsevier.com/locate/yjtbi

The disposition of the LZCC protein residues in wenxiang diagram provides new insights into the protein–protein interaction mechanism

Guo-Ping Zhou [a,b]

[a] Gordon Life Science Institute, 13784 Torrey Del Mar Drive, San Diego, CA 92130, USA
[b] Department of Chemistry, North Carolina State University, Raleigh, NC 27695, USA

ARTICLE INFO

Article history:
Received 10 February 2011
Received in revised form
28 April 2011
Accepted 7 June 2011
Available online 22 June 2011

Keywords:
Wenxiang diagram
Leucine zipper coiled-coil structure
NMR spectroscopy
Protein–protein interaction
cGMP-dependent protein kinase I

ABSTRACT

Wenxiang diagram is a new two-dimensional representation that characterizes the disposition of hydrophobic and hydrophilic residues in α-helices. In this research, the hydrophobic and hydrophilic residues of two leucine zipper coiled-coil (LZCC) structural proteins, cGKIα$^{1-59}$ and MBS$_{CT35}$ are dispositioned on the wenxiang diagrams according to heptad repeat pattern (**abcdefg**)$_n$, respectively. Their wenxiang diagrams clearly demonstrate that the residues with same repeat letters are laid on same side of the spiral diagrams, where most hydrophobic residues are positioned at **a** and **d**, and most hydrophilic residues are localized on **b**, **c**, **e**, **f** and **g** polar position regions. The wenxiang diagrams of a dimetric LZCC can be represented by the combination of two monomeric wenxiang diagrams, and the wenxiang diagrams of the two LZCC (tetramer) complex structures can also be assembled by using two pairs of their wenxiang diagrams. Furthermore, by comparing the wenxiang diagrams of cGKIα$^{1-59}$ and MBS$_{CT35}$, the interaction between cGKIα$^{1-59}$ and MBS$_{CT35}$ is suggested to be weaker. By analyzing the wenxiang diagram of the cGKIα$^{1-59}$·MBS$_{CT42}$ complex structure, most affected residues of cGKIα$^{1-59}$ by the interaction with MBS$_{CT42}$ are proposed at positions **d**, **a**, **e** and **g** of the LZCC structure. These findings are consistent with our previous NMR results. Incorporating NMR spectroscopy, the wenxiang diagrams of LZCC structures may provide novel insights into the interaction mechanisms between dimeric, trimeric, tetrameric coiled-coil structures.

1. Introduction

Coiled coil (CC) structural proteins usually contain a repeated pattern of nonpolar and charged amino-acid residues, referred to as a heptad repeat, which is denoted (abcdefg)$_n$. Where the positions for **a** and **d** are predominantly hydrophobic, often being occupied by leucine, isoleucine, or valine, and the positions at **b**, **c**, **e** and **g** are typically charged or polar (Chambers, et al., 1990; Crick, 1952; Hartmann et al., 2009; Lupas and Gruber, 2005; Surks, et al., 1999). It has been known that many CC type proteins are involved in important biological functions such as the regulation of gene expression. Representive examples include the oncoproteins c-fos and jun, and the muscle protein tropomyosin (Hartshorne, 1997; Hartshorne and Hirano, 1999; O'Shea et al., 1989; Surks and Mendelsohn, 2003).

Usually, a leucine zipper (LZ) structure is made up of two α-helical segments of a protein; it has leucines and/or isoleucines facing each other along the length of the helices, allowing them to dimerize and form a symmetric interface that can bind to the DNA on both sides of the double helix (Lupas and Gruber, 2005) or other proteins. As a three-dimensional structural motif, LZ structures are widely found in both eukaryotic and prokaryotic regulatory proteins (Baker et al., 2005; Rybalkin et al., 2002; Schlossmann et al., 2000; Surks, et al., 1999). The protein's domain possessing LZ motif usually is a CC structure. Thus this kind of protein is also referred as leucine zipper coiled-coil (LZCC) structural proteins. Evidences that the proteins of Leucine Zipper sequences belong to coiled-coil structures have been reported by many workers (O'Shea et al., 1989; Surks, et al., 1999; Surks and Mendelsohn, 2003).

Previous studies have shown that both cGMP-dependent protein kinase I, cGKIα$^{1-59}$ and the C-terminal 180 amino acids (residues 929–970) of the myosin binding subunit (MBS) of the myosin light-chain phosphatase (PPlM), MBS$_{CT180}$ contain LZCC domains. cGKIα$^{1-59}$ functions in the nitric oxide (NO) mediated relaxation of vascular smooth muscle (Lincoln, 1994). The cyclic GMP-mediated vascular smooth muscle cell relaxation is characterized by both a reduction of intracellular calcium concentration and by activation of PP1M, and thus results in sensitivity reduction of the contractile apparatus to intracellular calcium (Lincoln, 1994; Morgan and Morgan, 1984; Surks et al., 1999). The state of contraction or relaxation of vascular smooth muscle cells is closely coupled to phosphorylation and dephosphorylation of the regulatory myosin light chain, which is in part regulated by the binding of cGK1α to MBS of the PP1M. The disruption of the cGKIα-MBS interaction impairs cGMP-mediated dephosphorylation of myosin light chain, the critical determinant of smooth muscle cell contractile state

E-mail address: gzhou2@ncsu.edu

0022-5193/$ - see front matter © 2011 Elsevier Ltd. All rights reserved.
doi:10.1016/j.jtbi.2011.06.006

(Nakamura et al., 2007). More recently, the specific interaction between cGKIα$^{1-59}$ and MBS$_{CT42}$ (residues 929–1070), the C-terminal 42 amino acids of MBS protein has been further confirmed by NMR, biochemical and other biophysical methods such as glutathione S-transferase pulldown experiments, chemical cross-linking, size exclusion chromatography, circular dichroism, and isothermal titration calorimetry (Sharma et al., 2008; Zhou, 2011). These results further supported that the interaction between the cGKIα and MBS proteins actually is that between the LZCC of cGKIα$^{1-59}$ and the LZCC of MBSCT42.

In view of this, the present study was initiated in an attempt to utilize wenxiang diagram to characterize the LZCC domains of both cGKIα$^{1-59}$ and the LZCC of MBS$_{CT42}$. It has been known that many α-helices in proteins are amphiphilic, i.e., formed by the hydrophobic and hydrophilic amino acids according to a special order along the helix chain (Mercier et al., 1998; Schnell et al., 2005; Zhou, 2011). Besides, it has also been known that different types of proteins have different amphiphilic features, corresponding to different hydrophobic and hydrophilic order patterns (Chou, 2005; Kurochkina, 2010). As summarized in an article in Wikipedia (http://en.wikipedia.org/wiki/Alpha_helix, 2010), the wenxiang diagram (Chou et al., 1997) has the following advantages: (1) able to show the relative locations of the amino acids in an alpha-helix regardless how long it is; (2) able to indicate the direction of an alpha-helix; and (3) having the capacity to provide more information about each of the constituent amino acid residues in an α-helix. With these features, the wenxiang diagram can provide an easily visualizable picture in a 2D space for clearly characterizing the disposition of amphiphilic helices in proteins.

Using graphical approaches to study biological problems can provide an intuitive picture or useful insights for helping analyzing complicated mechanisms in these systems, as demonstrated by many previous studies on a series of important biological topics, such as enzyme-catalyzed reactions (Andraos, 2008; Chou, 1980, 1981, 1989; Chou and Forsen, 1980; Cornish-Bowden, 1979; King and Altman, 1956; Myers and Palmer, 1985; Zhou and Deng, 1984), protein folding kinetics and folding rates (Chou, 1990; Chou and Shen, 2009), inhibition of HIV-1 reverse transcriptase (Althaus et al., 1993a, 1993b, 1993c), inhibition kinetics of processive nucleic acid polymerases and nucleases (Chou et al., 1994), drug metabolism systems (Chou, 2010), analysis of DNA sequence (Xie and Mo, 2011; Yu et al., 2009), and protein sequence evolution (Wu et al., 2010). Moreover, graphical methods have been utilized to deal with complicated network systems (Gonzalez-Diaz et al., 2009; Munteanu et al., 2009) and identify the hub proteins from complicated network systems (Shen et al., 2010). Recently, the "cellular automaton image" (Wolfram 1984, 2002) has also been applied to study hepatitis B viral infections (Xiao et al., 2006), HBV virus gene missense mutation (Xiao et al., 2005a), and visual analysis of SARS-CoV (Wang et al., 2005), as well as representing complicated biological sequences (Xiao et al., 2005b) and helping to identify various protein attributes (Xiao et al., 2009, 2010). The present study was initiated in an attempt to use the elegant wenxiang diagram (Chou et al., 1997) to investigate protein–protein interactions in hope to gain useful insights for understanding some of their subtle action mechanisms. Because LZ and CC proteins have amphiphilic α-helical feature, it may be rewarding to use wenxiang diagram to investigate the disposition of their hydrophobic and hydrophilic residues. Our results will indicate that the heptad repeat and disposition of all residues in both cGKIα$^{1-59}$ and MBS$_{CT42}$ can be clearly displayed using the wenxiang diagrams. Furthermore, the specialties of the interaction between cGKIα$^{1-59}$ and MBS$_{CT42}$, could also be analyzed qualitatively by the wenxiang diagrams, and the dispositions of some key residues of cGKIα$^{1-59}$ in the wenxiang diagrams are basically consistent with our previous NMR experimental results (Sharma et al., 2008).

2. Materials and methods

2.1. The sequences of cGKI$^{\alpha 1-59}$ (residues 12–59) and MBS$_{CT42}$ (residues 936–970) proteins

The sequence of cGKIα$^{1-59}$ is

T^{1}SELEEDFAK^{10}ILMLKEERIK^{20}ELEKRLSEKE^{30}EEIQELKRKL^{40} HKCQSVLPVP^{50}STHIGPRTT^{59}.

The sequence of MBS$_{CT42}$ protein is

S^{929}TD^{931}FKKLY^{936}EQILA^{941}ENEKLKAQLHDTNMELTDL KLQ LEKATQR^{970}.

The coiled-coil predictions of the heptad repeat region were made using the programs COILS (Lupas et al., 1991; Berger et al., 1995).

2.2. Ensemble principle of wenxiang diagram of a coiled-coil dimmer

It has been clearly known that all amphiphilic helical proteins, with most hydrophobic residues being distinctly distributed in one-half of each wenxiang diagram, and most hydrophilic residues being distributed in the other half (Hartshorne., 1997; Sharma et al., 2008). Thus, the wenxiang diagrams of any LZCC structures should have similar characteristics. The hydrophobicity-weighed ($w^{+}(i)$) and hydrophilicity-weighed ($w^{-}(i)$) contributions of each residue, and hydrophobic and hydrophilic centroids of each α-helix can be determined by the wenxiang diagram coordinate system (Hartshorne, 1997). Furthermore, the inclination angle Ω, which is defined as the angle formed by the axis of the helix and its projected line on the plane S (Fig. 1) can be calculated using the following equation:

$$\Omega = \sin^{-1}[C_3^*/(C_2^{*2}+C_2^{*2}+C_3^{*2})^{-1/2}] \quad (1)$$

where C_1^*, C_2^*, and C_3^* are directly related to the hydrophobic atom coordinate system (x_o^+, y_o^+, z_o^+), hydrophilic atom coordinate system (x_o^-, y_o^-, z_o^-), hydrophobicity-weighed $w^+(i)$, and hydrophilicity-weighed $w^-(i)$ (Hartshorne, 1997).

According to the ensemble principle of wenxiang diagram, an α-helix can be viewed as a two-dimensional diagram generated by

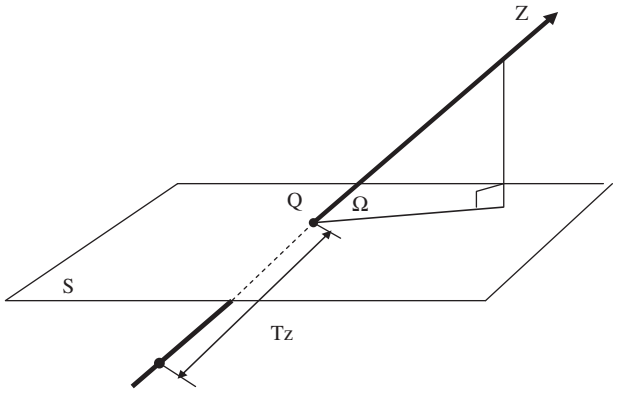

Fig. 1. Schematic drawing showing the inclination angle Ω and the intercept T_z of the interfacial plane *S*. *Q* is the intersection point of the helix axis *z* with the interfacial plane *S*. As shown in the figure, Ω is the angle between the helix axis *Z* and its projection on the plane *S*, whereas T_z is the distance from the projection of the frst C$^{\alpha}$ on the helix axis to Q (Hartshorne, 1997).

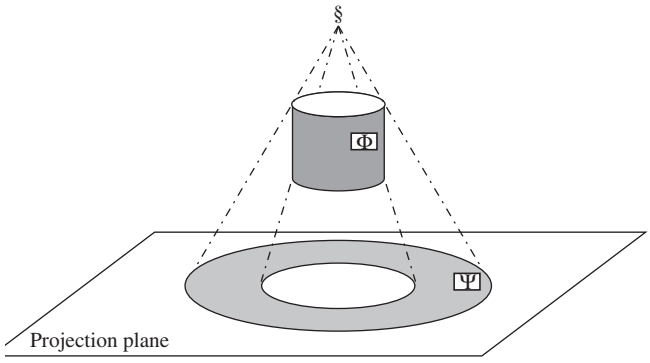

Fig. 2. Conical projection of a hollow cylinder Φ onto a plane perpendicular to the cylinder. The dot-dash lines (— · — · —) represent the radiating lines from the apex §. The distance § from the projection plane is arbitrary and is chosen to ensure that the resulting projection graph clearly portrays the relevant information. The image of the hollow cylinder on the projection plane is the ring ψ.

its conical projection (Fig. 2), where the projected image of a hollow cylinder Φ onto a plane perpendicular to it by conical projection will become a ring ψ. The outer and inner circles of the ring ψ correspond to the top and bottom circles of the hollow cylinder, respectively. Thus, the projected image of a helix could be viewed as a planar spiral with a continuous varying radius. If a helical COOH-terminal is close to its projected plane, and NH_2-terminal is far away the plane, the COOH-terminal of the helix lies near the center of the projected plane, and NH_2-terminal lies at the outer rim of the diagram. The disposition of a coiled-coil dimmer could be expressed by a pair of two-dimensional diagrams, i.e., two same monomer wenxiang diagrams.

3. Results and discussion

3.1. Distribution characteristics of the residues of cGKIα$^{1-59}$ and MBS$_{CT35}$ in the wenxiang diagrams

In previous studies, we have used programs COILS (Lupas, et al., 1991) to predict the coiled-coil region in cGKIα$^{1-59}$ domain, which is from the residue L12 through residue H53. This result has been confirmed by the analysis of our NMR relaxation data and RDC data (Schnell et al., 2005). This domain contains a repeating pattern of amino acids **a**, **b**, **c**, **d**, **e**, **f**, and **g** (Fig. 3A). Thus, the monomer structure of cGKIα$^{1-59}$ could be characterized by a wenxiang diagram. Where each residue of the denoted repeating amino acids $(abcdefg)_n$ in Fig. 3B is represented by a circle and repeated letters **a**, **b**, **c**, **d**, **e**, **f**, and **g**, respectively. It is clearly shown with the wenxiang diagram that the residues with same letters are laid on same side of the spiral diagram, and most hydrophobic residues are positioned on **a/d** region except Lysine 15 and 29 (Fig. 3B).

Because a LZ domain must be a typical amphiphilic helix, i.e., part of the helix flank is dominated by hydrophobic residues and the other part by hydrophilic residues, their inclination angles are all very close to 0°, which is fully consistent with the requirement of minimum free energy in a amphiphilic helical system (Hartshorne, 1997).

It has been suggested that a critical region responsible for interacting with cGKIα$^{1-59}$ is another LZ coiled-coil domain, which is located within the C-terminal 100 amino acids (residues 930–1030) of the MBS (Baker et al., 2005; Lincoln, 1994). This region has been further confirmed to be MBS$_{CT42}$, the C-terminal 42 amino acids (residues 929–970) of the MBS protein by our NMR data (Sharma et al., 2008). Actually, according to our pair coil analysis, the LZCC domain with the highest probability (1.0) should be the C-terminal 35 amino acids of the MBS (MBS$_{CT35}$), which contains a repeating pattern of amino acids **a**, **b**, **c**, **d**, **e**, **f**, and **g** from residues

A

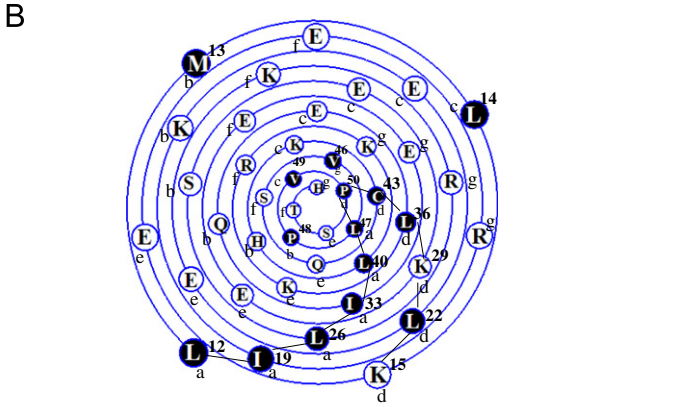

B

Fig. 3. The Sequences containing the heaptad repeat pattern (abcdefg)n in LZCC domains of cGKIα$^{1-59}$ (A), and the monomer wenxiang diagram of cGKIα$^{1-59}$ (B). The each residue position in a heptad repeat was labeled using **a**, **b**, **c**, **d**, **e**, **f**, and **g**, respectively. In B, all positions **a/d** are connected by the solid line, and a hydrophobic residues is denoted by filled circle with its code symbol in white, whereas a hydrophilic residue is denoted by an open circle with its code symbol in black.

A

B

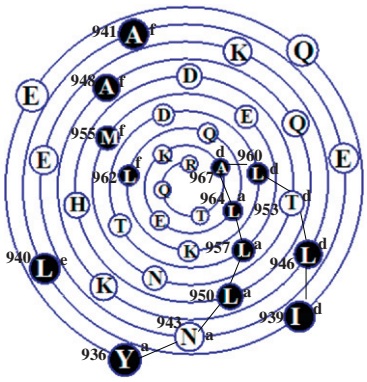

Fig. 4. The Sequences containing the heaptad repeat pattern (abcdefg)n in LZCC domains of MBS$_{CT35}$ (A), and the monomer wenxiang diagram of MBS$_{CT35}$ (B). The each residue position in a heptad repeat was labeled using **a**, **b**, **c**, **d**, **e**, **f**, and **g**, respectively. In B, all positions **a/d** are connected by the solid line, and a hydrophobic residues is denoted by filled circle with its code symbol in white, whereas a hydrophilic residue is denoted by an open circle with its code symbol in black. Only the residues of position **a/d** and hydrophobic residues are labeled by the sequence number. The larger the radius an amino acid residue has in the spiral, the farther above the projection plane is the corresponding amino acid in the helix and vice versa.

936 to 970 (Fig. 4A). Because all residues of MBS$_{CT35}$ are included in MBS$_{CT42}$ domain, the interaction between it and cGKIα$^{1-59}$ has been confirmed by our biochemical and NMR data (Lincoln., 1994). According to this information, we obtained a wenxiang diagram of the monomer of MBS$_{CT35}$, where all residues with same letter are also distributed on the same side of the spiral wenxiang diagram (Fig. 4B). It can be seen from both Figs. 3 and 4B and that most nonpolar residues are localized on the hydrophobic **a/d** regions.

According to the calculated results for a number of proteins, the inclination angles for most helices therein are small ($|\Omega| < 25°$).

This suggests that driven by the free energy an amphiphilic helix will tend to seek its own arrangement in a protein such that approximately half of its face is buried in the protein, whereas the other half is exposed to the aqueous environment that surrounds the protein (Hartshorne, 1997). Thus, a coiled-coil dimmer structure can be further expressed by a combination of two identical two-dimensional wenxiang diagrams. The ensemble principle of such wenxiang diagram should observe the following rule: **a/d** region of one monomer wenxiang diagram must be faced to the **a/d** region of another identical monomer wenxiang diagram. Because most hydrophobic residues are localized at the **a/d** positions, the approach to each other between the two monomer's **a/d** regions should be helpful for the formation of a stable coiled-coil dimmer structure due to the hydrophobic interactions of the nonpolar residues between the two **a/d** regions. According to such an ensemble rule, the wenxiang diagrams of the cGKIα$^{1-59}$ dimmer were assembled in Fig. 5A. Where most hydrophobic side chains of leucine and isoleucine in positions **a** and **d**, and two side chains of lysine (K15 and K29) in position **d** should be clearly displayed on the nearest neighbor region between the two wenxiang diagrams. This observation has been verified by our 3D structure of cGKIα$^{1-59}$ (Fig. 6) based on the previous NMR experimental data (Surks and Mendelsohn, 2003).

As shown in Fig. 5, the hydrophobic side chains of leucine and isoleucine in positions **a** and **d** are shown in green, and the two side chains of K15 and K29 are in position **d** are shown in red. Similarly, the wensiang diagrams of MBS$_{CT35}$ dimer structure were also obtained according to the above the ensemble principle. As shown in Fig. 5B, the **a/d** position region of a monomer faces to the **a/d** position region of another monomer on the wenxiang

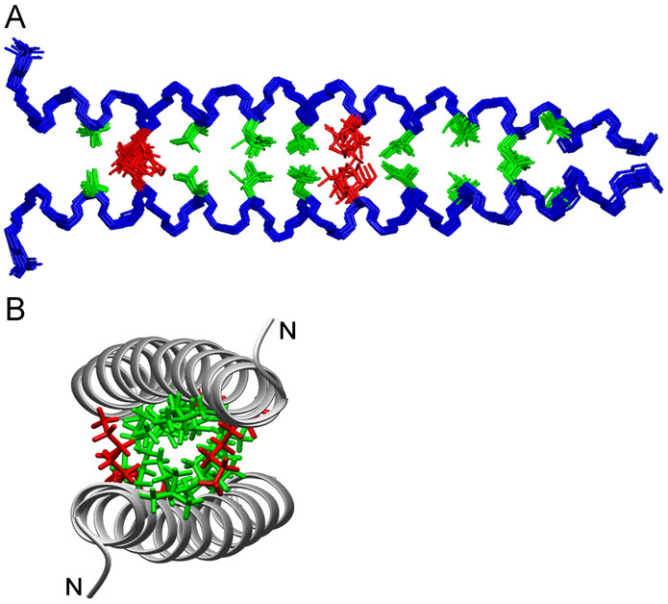

Fig. 6. 3D structure of LZCC domains of cGKIα$^{1-59}$. (A) Bundle of 20 refined parallel coiled-coil dimer structures with lowest RDC energies superimposed on the backbone heavy atoms (blue). The hydrophobic side chains of leucine and isoleucine in positions an and d are shown in green, and the two side chains of lysine which are in position d are shown in red. (B) End-on view from the N-terminus of a representative refined dimer. The backbone structure is shown as a ribbon diagram, and side chains are colored as in (A). (For interpretation of the references to color in this figure legend, the reader is referred to the web version of this article.)

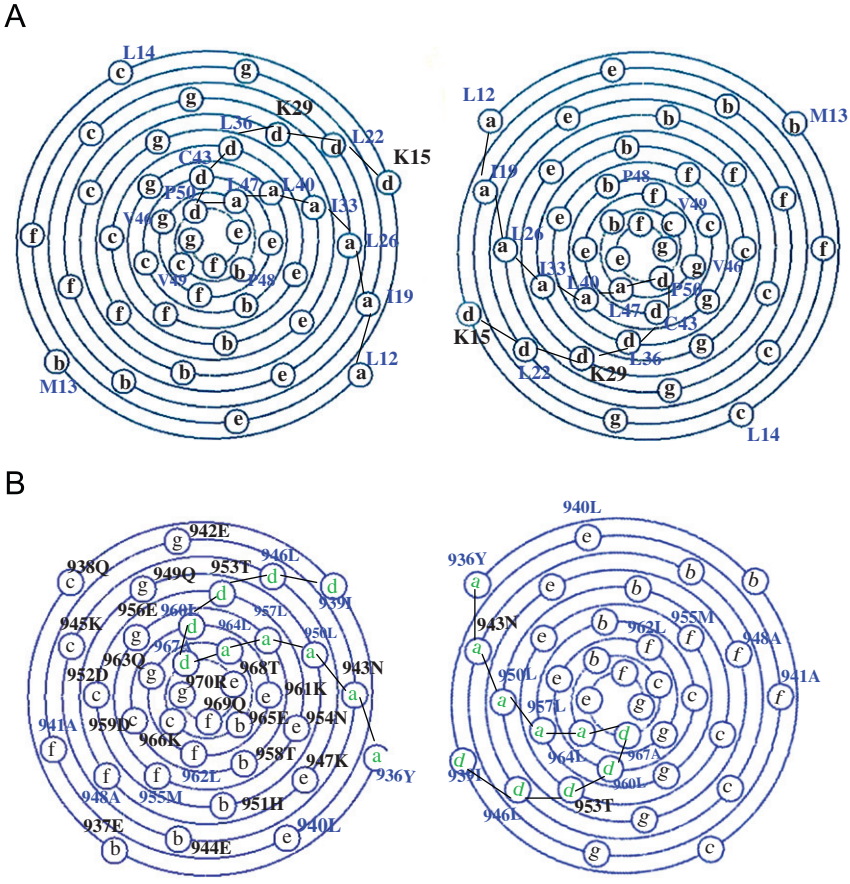

Fig. 5. The Wenxiang diagrams of two LZCC dimmers. (A) cGKIα$^{1-59}$ dimer; (B) MBS$_{CT35}$ dimer. All position a/d are connected by the solid line. The name and sequence numbers of all hydrophobic residues are labeled by blue. (For interpretation of the references to color in this figure legend, the reader is referred to the web version of this article.)

diagrams of MBS_{CT35} LZCC structure. In Fig. 5A, although the seven apolar residues (M13, L14, Y46, P48, V49, G55, and P56) of $cGKI\alpha^{1-59}$ localize the outside of the **a/d** position region, most of them are still close to the **a/d** region except residues M13 and L14. However, for the wenxiang diagrams of MBS_{CT35}, an interesting feature is that most apolar residues of outside the hydrophobic **a/d** position region such as 941 A, 948 A, 955 M and 962 L are located at position **f** (where usually are occupied by the hydrophilic residues) and are little far away from the hydrophobic **a/d** position region (Fig. 5B). These differences between Figs. 5A and B suggest that the either hydrophobic or hydrophilic interactions between $cGKI\alpha^{1-59}$ and MBS_{CT35} may be weaker due to the lack of the contributions of the more apolar residues near the **a/d** position region of MBS_{CT35}, or lack of the contributions of polar residues from **g, b, c,** and **e** positions of $cGKI\alpha^{1-59}$ This may explain why the molar ratio of the interaction between MBS_{CT42} and $cGKI\alpha^{1-59}$ has to be 2:1(Lincoln, 1994).

3.2. *Analysis of the interaction between $cGKI\alpha^{1-59}$ and MBS_{CT35} incorporating wenxiang diagrams and NMR data*

In order to determine whether an interaction exists between $cGKI\alpha^{1-59}$ and MBS_{CT42}, Figs. 5A and B were combined to form the wenxiang diagrams of a hexamer complex structure according to the molar ratio of $cGKI\alpha^{1-59}$ and MBS_{CT35} (1:2) (Fig. 7).

The ensemble of these combined wenxiang diagrams should be reasonable. Because most hydrophobic residues (position **a/d** regions, or nearby **a/d** regions) are buried inside the bundle and most hydrophilic residues are exposed to the aqueous environment that surrounds the $cGKI\alpha^{1-59}$• MBS_{CT42} hexamer complex. As shown in Fig. 7, the **a–e** position region of $cGKI\alpha^{1-59}$ is close to the **d–g** position region of MBS_{CT35}, and the **d–g** position regions of $cGKI\alpha^{1-59}$ is close to the **a–e** position regions of MBS_{CT35}. The all residues (E16, E23, E30, K37, Q44 and S51) at position **e** of $cGKI\alpha^{1-59}$ are all polar residues. In the other hand, all residues (942E, 949Q, 956E, 963Q and

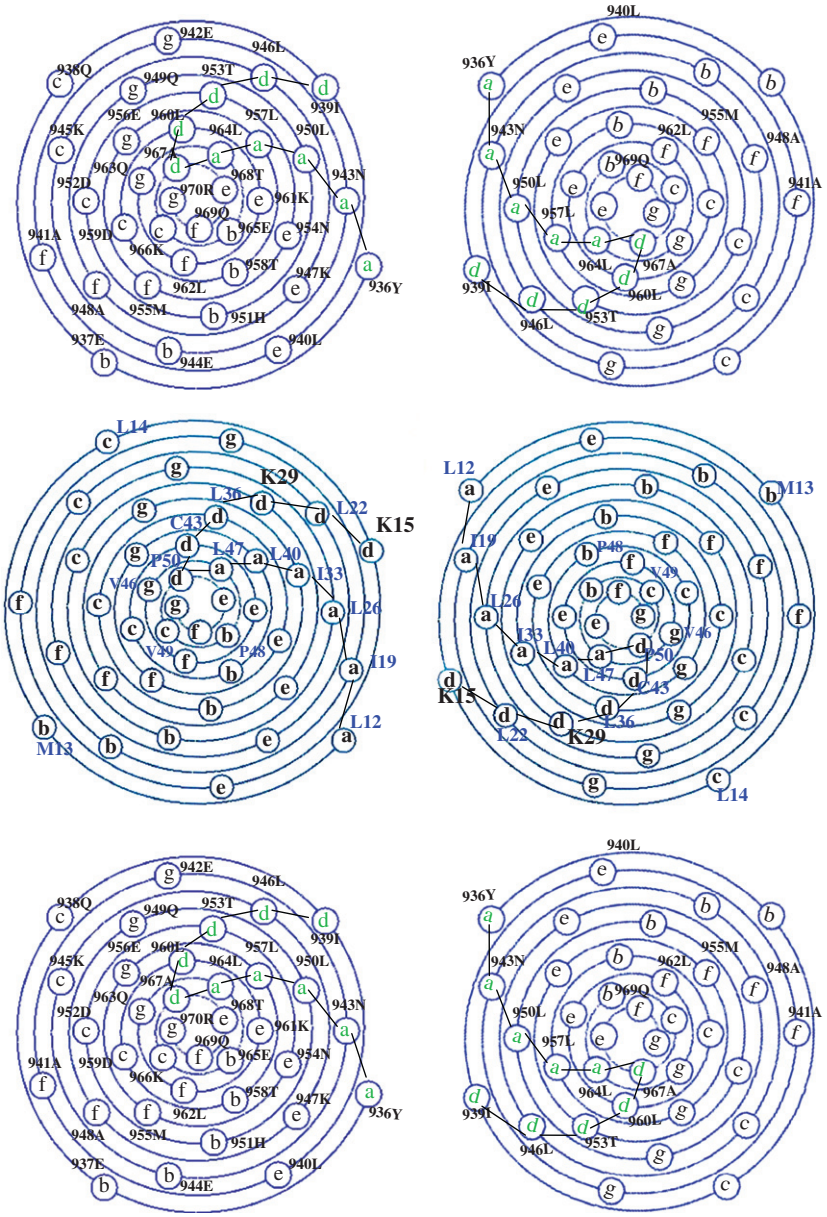

Fig. 7. The wenxiang diagrams of the hexamer complex structure of $cGKI\alpha^{1-59}$ (middle pair diagrams) and two MBS_{CT35} (the topper and lower pair diagrams). Where, the **a–e** region of one molecule is close to the **d–g** region of another molecule.

970R) at position **g** of MBS_{CT35} are also polar residues. According to the previous studies (Adamian and Liang, 2002), the salt bridge residue pairs of E–R may be formed between E16, E23, or E30 of $cGKI\alpha^{1-59}$ and 970R of MBS_{CT35}, and the salt bridge residue pairs of R–E may be formed between R37 of $cGKI\alpha^{1-59}$ and 942E or 956E of MBS_{CT35}. These salt bridges have high propensity for the interhelical polar-polar atomic contacts. In addition, other ionizable-polar residue pairs such as Q–R or R–Q (Q44–970R, or R37–949Q, or R37–963Q), and S–R (S51–970R) between $cGKI\alpha^{1-59}$ and MBS_{CT35} may also have high propensity to form the interhelical polar-polar interactions (Adamian, and Liang, 2002), Similarly, the all residues (R18, R25, E32, K39, and H53) at position **g** of $cGKI\alpha^{1-59}$ are all polar residues, and most residues (947K, 954N, 961K, and 968T) at position **e** of MBS_{CT35} are also polar residues. The ionzable-polar residue pairs such as R–N (R18–954N), or K-N (K39–954N), or H–T (H53–968T) between $cGKI\alpha^{1-59}$ and MBS_{CT35} may also be formed to contribute the interhelical polar-polar interactions.

Such ensemble of the wenxiang diagrams suggests that most affected residues of $cGKI\alpha^{1-59}$ and MBS_{CT35} might be at positions **d**, **a**, **e** and **g** of these two LZCC structures. This prediction has been supported by the previous NMR data (Lincoln, 1994; Sharma et al., 2008).

NMR spectroscopy is the preferred method for characterizing the structural details of protein–protein and protein-ligand interaction interfaces following complex formation in an aqueous environment (Chou et al., 1997). Our ^{15}N-^{1}H-HSQC titration data in which unlabeled MBS_{CT42} (not observable by ^{15}N-^{1}H-HSQC experiment) was titrated into $^{2}H/^{13}C/^{15}N$-labeled $cGKI\alpha^{1-59}$ support an interaction between $cGKI\alpha^{1-59}$ and MBS_{CT42}, which is illustrated by the changes in chemical shifts of the 5 residues (Leu^{36}, Lys^{37}, Leu^{40}, Ile^{54}, and Gly^{55}) as well as a significant decrease in peak intensity of the 8 residues (Leu^{22}, Ile^{33}, Leu^{36}, Lys^{37}, Lys^{39} , Leu^{40}, Cys^{43}, and Gln^{44}) of $cGKI\alpha^{1-59}$ (Lincoln, 1994). Taken together, these data identify that these 10 residues (Leu22, Ile 33, Leu36, Lys37, Lys 39, Leu40, Cys43, Gln44, Ile54, and Gly55) of $cGKI\alpha^{1-59}$ are most affected by the interaction with MBS_{CT42} (Lincoln, 1994). The seven residues of them are hydrophobic and only three for hydrophilic residues (Lys 37, Lys 39 and Gln44). Among these 10 residues, the three residues (I33, L40 and I54) at position **a**, the three residues (L22, L36 and C43) at position **d**, the two residues (K37 and Q44) at position **e**, the one residue (K39) at the position **g**, and the one residue (G55) at position **b** of $cGKI\alpha^{1-59}$ are most affected residues by the interaction with MBS_{CT42} (Lincoln, 1994). Thus, the previous NMR experimental data have supported above prediction based on above combined wensiang diagrams that most affected residues of $cGKI\alpha^{1-59}$ by the interaction with MBS_{CT35} might be at positions **d, a, e** and **g** of these two LZCC structures.

In addition, the residues which are localized at positions **c** and **f** (particularly for **f**) region of $cGKI\alpha^{1-59}$, are far away from the all position regions of MBS_{CT35} according to the wenxiang diagrams of $cGKI\alpha^{1-59}$• MBS_{CT35} complex. This means that most residues at position **c** and **f** regions are more exposed the outer of the complex, or exposed to the aqueous environment that surrounds the protein complex. These results suggest that the interactions between $cGKI\alpha^{1-59}$ and MBS_{CT35} come from the contribution of their hydrophobic residues at positions **a** and **d**, as well as the hydrophilic residues at position **g**.

Interestingly, these residues are localized on the same side of the helix or close to each other in the wenxiang diagram (Fig. 7). These characteristics further support our previous suggestion that these 10 residues are reasonably either within close proximity to and/or involved in the formation of the interaction interface (Lincoln, 1994). Based on similar data obtained in studies of F-actin interacting with skeletal myosin light chain 1 and ubiquitin hydrolase interacting with its native substrate, it is likely that these residues are within the interaction interface between these proteins although additional experiments evaluating the on/off rate of the interaction may are necessary (Naik et al., 2001; Sakamoto et al., 2005; Hutchings et al., 2003).

As has been previously identified for the GCN4 LZ, upon tetramer formation (pairing of two dimers) there is an increase in packing density within the intermolecular interface, which results in additional perturbation of residues within the **a**, **d**, **e**, **b** and **g** positions that is unlike the typical packing of the **a** and **d** side chains of isolated helices (Harbury et al., 1994). Interestingly several of the residues of $cGKI\alpha^{1-59}$ that are conformationally perturbed following the addition of MBS are within **a**, **d**, **e**, **g** and **b** positions of the repeating heptads layer (Fig. 7). In addition, the previous studies about the GCN4 tetramer LZ, an isoleucine zipper trimer of GCN4, the asialoglycoprotein receptor heterotetramer, and an extensive study of Crick's knobs-into-holes packing for 3-, 4- and 5-stranded structures have provided additional geometric, conformational packing information for generating this model (Harbury et al., 1993; 1994;1995; Walshaw and Woolfson, 2003). Moreover, in the crystal structure of the GCN4 trimer and tetramer the authors observe significant packing and numerous interactions between residues in the **a/d** hydrophobic interface and the hydrophilic residues at positions **e** and **g**, which and our $cGKI\alpha^{1-59}$• MBS_{CT42} complex wenxiang diagrams may be consistent and helpful for a better understanding the packing mechanism that present between the $cGKI\alpha^{1-59}$ LZCC domain and MBS_{CT42} LZCC motif.

4. Conclusion

Although many leucine zipper domains of proteins have been characterized by a heptad repeat of leucine residues in a helical wheel (Jones et al., 1992), the information thus provided about the α-helices and their lengths are very limited. If the helical wheel diagrams of a LZCC structure are used to represent two α-helices longer than 20 residues, they must crowd into a very limited space or overlap with each another, and will be difficult to be distincted from each other. It is particularly difficult to represent a LZCC-LZCC tetramer complex using four helical wheel diagrams. In contrast, the wenxiang diagrams can be used to represent two α-helixes regardless how long they are. Furthermore, wenxiang diagrams of LZCC structure can provide much more information about the physico-chemical features of the constituent amino acids as well as their distribution even for four-alpha-helix bundle with heptad repeat residues. Furthermore, our results also suggest that the wenxiang diagrams of a LZCC structure can be used to identify the key residues that play the most important role for its interaction with another LZCC protein. It is demonstrated through this study that wenxiang diagram holds a great potential in providing more information about each of the constituent amino acid residues in a heptads' repeat. Incorporated with NMR or other biological/biophysical experimental results, wenxiang diagram may provide useful insights into the 3D structural model of LZCC protein and the interaction mechanism between LZCC and LZCC proteins.

References

Adamian, L., Liang, J., 2002. Interhelical hydrogen bonds and spatial motifs in membrane proteins: polar clamps and serine zippers. Protein: Struct. Funct. Genet. 47, 209–218.

Althaus, I.W., Chou, J.J., Gonzales, A.J., Diebel, M.R., Chou, K.C., Kezdy, F.J., Romero, D.L., Aristoff, P.A., Tarpley, W.G., Reusser, F., 1993a. Kinetic studies with the nonnucleoside HIV-1 reverse transcriptase inhibitor U-88204E. Biochemistry 32, 6548–6554.

Althaus, I.W., Chou, J.J., Gonzales, A.J., Diebel, M.R., Chou, K.C., Kezdy, F.J., Romero, D.L., Aristoff, P.A., Tarpley, W.G., Reusser, F., 1993b. Steady-state kinetic studies with the non-nucleoside HIV-1 reverse transcriptase inhibitor U-87201E. J. Biol. Chem. 268, 6119–6124.

Althaus, I.W., Gonzales, A.J., Chou, J.J., Diebel, M.R., Chou, K.C., Kezdy, F.J., Romero, D.L., Aristoff, P.A., Tarpley, W.G., Reusser, F., 1993c. The quinoline U-78036

is a potent inhibitor of HIV-1 reverse transcriptase. J. Biol. Chem. 268, 14875–14880.
Andraos, J., 2008. Kinetic plasticity and the determination of product ratios for kinetic schemes leading to multiple products without rate laws: new methods based on directed graphs. Can. J. Chem. 86, 342–357.
Baker, P.R.S., Lin, Y., Schopfer, F.J., Woodcock, S.R., Groeger, A.L., Batthyany, C., Sweeney, S., Long, M.H., Iles, K.I., Baker, M.L.S., Branchaud, B.P., Chen, Y.E., Freeman, B.A., 2005. Fatty acid transduction of nitric oxide signaling: multiple nitrated unsaturated fatty acid derivatives exist in human blood and urine and serve as endogenous PPAR ligands. J. Biol. Chem. 280 (51), 42475–42646.
Berger, B., Wilson, D.B., Wolf, E., Tonchev, T., Milla, M., Kim, P.S., 1995. Predicting coiled coils by use of pairwise residue correlations. Proc. Natl. Acad. Sci. USA 92, 8259–8263.
Chou, K.C., 1980. A new schematic method in enzyme kinetics. Eur. J. Biochem. 113, 195–198.
Chou, K.C., Forsen, S., 1980. Graphical rules for enzyme-catalyzed rate laws. Biochem. J. 187, 829–835.
Chou, K.C., 1981. Two new schematic rules for rate laws of enzyme-catalyzed reactions. J. Theor. Biol. 89, 581–592.
Chou, K.C., 1989. Graphic rules in steady and non-steady enzyme kinetics. J. Biol. Chem. 264, 12074–12079.
Chou, K.C., 1990. Review: applications of graph theory to enzyme kinetics and protein folding kinetics. steady and non-steady state systems. Biophys. Chem. 35, 1–24.
Chou, K.C., Kezdy, F.J., Reusser, F., 1994. Review: Steady-state inhibition kinetics of processive nucleic acid polymerases and nucleases. Anal. Biochem. 221, 217–230.
Chou, K.C., Zhang, C.T., Maggiora, G.M., 1997. Disposition of amphiphilic helices in heteropolar environments. Proteins: Struct. Funct. Genet. 28, 99–108.
Chou, K.C., 2005. Using amphiphilic pseudo amino acid composition to predict enzyme subfamily classes. Bioinformatics 21, 10–19. doi:10.1093/bioinformatics/b.
Chou, K.C., Shen, H.B., 2009. FoldRate: a web-server for predicting protein folding rates from primary sequence 3, 31–50Open Bioinf. J. 3, 31–50 (openly accessible at 〈http://www.bentham.org/open/tobioij/〉).
Chou, K.C., 2010. Graphic rule for drug metabolism systems. Curr. Drug Metab. 11, 369–378.
Chambers, P., Pringle, C.R., Easton, A.J., 1990. Heptad repeat sequences are located adjacent to hydrophobic regions in several types of virus fusion glycoproteins. J. Genet. Virol. 71, 3075–3080 (Printed in Great Britain).
Crick, F.H., 1952. Is alpha-keratin a coiled coil? Nature 170 (4334), 882–883.
Cornish-Bowden, A., 1979. Fundamentals of Enzyme Kinetics. Butterworths, London (Chapter 4).
Gonzalez-Diaz, H., Perez-Montoto, L.G., Duardo-Sanchez, A., Paniagua, E., Vazquez-Prieto, S., Vilas, R., Dea-Ayuela, M.A., Bolas-Fernandez, F., Munteanu, C.R., Dorado, J., Costas, J., Ubeira, F.M., 2009. Generalized lattice graphs for 2D-visualization of biological information. J. Theor. Biol. 261, 136–147.
Harbury, P.B., Zhang, T., Kim, P.S., Alber, T., 1993. A switch between two-, three., freedom: structure prediction for coiled coils. Biochemistry 262, 1401–1406 9223408-8412.
Harbury, P.B., Kim, P.S., Alber, T., 1994. Crystal structure of an isoleucine-zipper. Nature 371 (6492), 80–83. doi:10.1038/371080a0 PMID 8072533.
Hartshorne, D.J., 1997. Interactions of the subunits of smooth muscle myosin phosphatase. J. Biol. Chem. 272, 3683.
Hartshorne, D.J., Hirano, K., 1999. Review interactions of protein phosphatase type 1, with a focus on myosin phosphatase. Mol. Cell. Biochem. 190, 79–84.
Hartmann, M.D., Ridderbusch, O., Zeth, K., Albrecht, R., Testa, O., Woolfson, D.N., Sauer, G., Dunin-Horkawicz, S., Lupas, A.N., Alvarez, B.H., 2009. A coiled-coil motif that sequesters ions to the hydrophobic core. Proc. Natl. Acad. Sci. USA 106 (40), 16950–16955.
Hutchings, N.J., Clarkson, N., Chalkley, R., Barclay, A.N., Brown, M.H., 2003. Linking the T cell surface protein CD2 to the actin-capping protein CAPZ via CMS and CIN85. J. Biol. Chem. 278, 22396–22403.
Jones, M.K., Anantharamaiah, G.M., Segrest, J.P., 1992. Computer programs to identify and classify amphipathic a helical domains. J. Lipid Res. 33, 287–296.
King, E.L., Altman, C., 1956. A schematic method of deriving the rate laws for enzyme-catalyzed reactions. J. Phys. Chem. 60, 1375–1378.
Kurochkina, N., 2010. Helix–helix interactions and their impact on protein motifs and assemblies. J. Theor. Biol. 264, 585–592.
Lincoln, T.M., 1994. Cyclic GMP: Biochemistry. Physiology and Pathophysiology (R. G. Landes Company, Austin, TX, pp. 97–115.
Lupas, A., Van, D.M., Stock, J., 1991. Science 252, 1162–1164.
Lupas A.N., Gruber M., 2005. The structure of alpha-helical coiled coils. Adv. Protein Chem. 70:37–78.
Mercier, C., Cesbron-Delauw, M.F., Sibley, L.D., 1998. The amphipathic alpha helices of the Toxoplasma protein GRA2 mediate post-secretory membrane association. J. Cell Sci. 111, 2171–2180.
Morgan, J.P., Morgan, K.G., 1984. J. Physiol. (London) 357, 539.
Munteanu, C.R., Magalhaes, A.L., Uriarte, E., Gonzalez-Diaz, H., 2009. Multi-target QPDR classification model for human breast and colon cancer-related proteins using star graph topological indices. J. Theor. Biol. 257, 303–311.
Myers, D., Palmer, G., 1985. Microcomputer tools for steady-state enzyme kinetics. Bioinformatics (Orig.: Comput. Appl. Biosci.) 1, 105–110.
Naik, R.R., Kirkpatrick, S.M., Stone, M.O., 2001. The thermostability of an α-helical coiled-coil protein and its potential use in sensor applications. Biosens. Bioelectron. 16 (9-12), 1051–1057.
Nakamura, I.K., Koga, Y., Sakai, H., Homma, K., Mitsuo, I., 2007. cGMP-dependent relaxation of smooth muscle is coupled with the change in the phosphorylation of myosin phosphatase. Circul. Res. 101, 712.
O'Shea, E.K., Rutkowski, R., Kim, P. S., P.S., 1989. Evidence that the leucine zipper is a coiled coil. Science 243, 538–542.
Rybalkin, S.D., Rybalkina, I.G., Feil, R., Hofmann, F., Beavo, J.A., 2002. Regulation of cGMP-specific phosphodiesterase (PDE5) phosphorylation in smooth muscle cells. J. Biol. Chem. 277, 3310–3317.
Sakamoto, R., Byrd, S., Brown, D.T., Hisamoto, H.M., Matsumoto, N., Jin, Y., K., 2005. The Caenorhabditis elegans UNC-14 RUN domain protein binds to the kinesin-1 and UNC-16 complex and regulates synaptic vesicle localization. Mol. Biol. Cell 16, 483–496.
Schlossmann, J., Ammendola, A., Ashman, K., Zong, X., Huber, A., Neubauer, G., Wang, G.X., Allescher, H.D., Kroth, M., Wilm, M., Hof-mann, F., Ruth, P., 2000. Regulation of intracellular calcium by a signalling complex of IRAG, IP3 receptor and cGMP kinase ibeta. Nature 404, 197–201.
Schnell, J.R., Zhou, G.-P., Zweckstetter, M., Rigby, A.C., Chou, J.J., 2005. Rapid and accurate structure determination of coiled-coil domains using NMR dipolar couplings: application to cGMP-dependent protein kinase Ia. Prot. Sci. 14 (9), 2421–2428.
Sharma, A.K., Zhou, G.P.J., Kupferman, J., Surks, H.K., Eva N. Christensen, E.N., Chou, J.J., Mendelsohn, M.E., Rigby, A.C., 2008. Probing the interaction between the coiled coil leucine zipper of cgmp-dependent protein kinase and the C terminus of the myosin binding subunit of the myosin light chain phosphatase. J. Biol. Chem. 283 (47), 32860–32869.
Shen, Y.Z., Ding, Y.S., Gu, Q., Chou, K.C., 2010. Identifying the hub proteins from complicated membrane protein network systems. Med. Chem. 6, 165–173.
Surks, H.K., Mochizuki, N., Kasai, Y., Georgescue, S.P., Tang, K.M., Ito, M., Lincoln, T.M., Mendelsohn, M.E., 1999. Science 286, 1583–1587.
Surks, H.K., Mendelsohn, M.E., 2003. Dimerization of cGMP-dependent protein kinase 1[alpha] and the myosin-binding subunit of myosin phosphatase: role of leucine zipper domains. Cell. Signal. 15, 937–944.
Wang, X.Y., Yang, J., Zhu, Y.S., Chou, K.C., 2005. A new nucleotide-composition based fingerprint of SARS-CoV with visualization analysis. Med. Chem. 1, 39–47.
Walshaw, J., Woolfson, D.J., 2003. Extended knobs-into-holes packing in classical and complex coiled-coil assemblies. J. Struct. Biol. 144, 349–361.
Wolfram, S., 1984. Cellular automation as models of complexity. Nature 311, 419–424.
Wolfram, S., 2002. A New Kind of Science. Wolfram Media Inc, Champaign, IL.
Wu, Z.C., Xiao, X., Chou, K.C., 2010. 2D-MH: A web-server for generating graphic representation of protein sequences based on the physicochemical properties of their constituent amino acids. J. Theor. Biol. 267, 29–34.
Xiao, X., Shao, S.H., Chou, K.C., 2006. A probability cellular automaton model for hepatitis B viral infections. Biochem. Biophys. Res. Commun. 342, 605–610.
Xiao, X., Wang, P., Chou, K.C., 2009. GPCR-CA: A cellular automaton image approach for predicting G-protein-coupled receptor functional classes. J. Comput. Chem. 30, 1414–1423.
Xiao, X., Wang, P., and Chou, K.C., 2010. Quat-2 L: a web-server for predicting protein quaternary structural attributes. Mol. Divers., doi:10.1007/s11030-010-9227-8.
Xiao, X., Shao, S., Ding, Y., Huang, Z., Chen, X., Chou, K.C., 2005a. An application of gene comparative image for predicting the effect on replication ratio by HBV virus gene missense mutation. J. Theor. Biol. 235, 555–565.
Xiao, X., Shao, S., Ding, Y., Huang, Z., Chen, X., Chou, K.C., 2005b. Using cellular automata to generate image representation for biological sequences. Amino Acids 28, 29–35.
Xie, G., Mo, Z., 2011. Three 3D graphical representations of DNA primary sequences based on the classifications of DNA bases and their applications. J. Theor. Biol. 269, 123–130.
Yu, J.F., Sun, X., Wang, J.H., 2009. TN curve: a novel 3D graphical representation of DNA sequence based on trinucleotides and its applications. J. Theor. Biol. 261, 459–468.
Zhou, G.P., Deng, M.H., 1984. An extension of Chou's graphical rules for deriving enzyme kinetic equations to system involving parallel reaction pathways. Biochem J 222, 169–176.
Zhou, G.P., 2011. The structural determinations of the leucine zipper coiled-coil domains of the cGMP-dependent protein kinase I and its interaction with the myosin binding subunit of the myosin light chains phosphase. Protein Peptide Lett. 50, 1162–1173.